Noise spectroscopy of a quantum-classical environment with a diamond qubit

S. Hernández-Gómez, F. Poggiali, P. Cappellaro, and N. Fabbri

Noise spectroscopy of a quantum-classical environment with a diamond qubit

S. Hernández-Gómez,[1,2] F. Poggiali,[1,2] P. Cappellaro,[1,3] and N. Fabbri[1,2,*]

[1]*LENS European Laboratory for Non linear Spectroscopy, Università di Firenze, I-50019 Sesto Fiorentino, Italy*
[2]*CNR-INO Istituto Nazionale di Ottica del Consiglio Nazionale delle Ricerche, I-50019 Sesto Fiorentino, Italy*
[3]*Department of Nuclear Science and Engineering, Massachusetts Institute of Technology, Cambridge, MA 02139*

Knowing a quantum system's environment is critical for its practical use as a quantum device. Qubit sensors can reconstruct the noise spectral density of a classical bath, provided long enough coherence time. Here we present a protocol that can unravel the characteristics of a more complex environment, comprising both unknown coherently coupled quantum systems, and a larger quantum bath that can be modeled as a classical stochastic field. We exploit the rich environment of a Nitrogen-Vacancy center in diamond, tuning the environment behavior with a bias magnetic field, to experimentally demonstrate our method. We show how to reconstruct the noise spectral density even when limited by relatively short coherence times, and identify the local spin environment. Importantly, we demonstrate that the reconstructed model can have predictive power, describing the spin qubit dynamics under control sequences not used for noise spectroscopy, a feature critical for building robust quantum devices. At lower bias fields, where the effects of the quantum nature of the bath are more pronounced, we find that more than a single classical noise model are needed to properly describe the spin coherence under different controls, due to the back action of the qubit onto the bath.

I. INTRODUCTION

Characterizing the interaction of a qubit with its environment is critical to realize robust quantum devices. A full understanding of the qubit environment enables developing effective strategies against decoherence, including optimized dynamical decoupling (DD) sequences[1,2] and quantum error correction codes[3]. Moreover, part of the environment might display coherent coupling to the qubit and thus provide an additional resource to enhance its computational or sensing performance[4–6].

Fortunately, the qubit itself is a sensitive probe of its local environment. In addition to T_2^* relaxometry[7–10] and spin locking schemes[11,12], the most common and powerful noise spectroscopy methods[13–17] rely on the systematic analysis of the sensor decoherence under sets of DD control sequences[18–21]. Periodic DD sequences realize narrow frequency filters that select only a specific noise contribution, while canceling all other interactions. This method has been used for noise identification with spin qubits in diamond[22–24], superconductive flux qubits[25], trapped ions[26], and nanoelectronic devices[27]. While the filter function approach has been extended in some cases to more complex and quantum baths[2,28], most of these noise spectroscopy methods usually assume the environment to be a classical stochastic bath[16,21,29]. In addition these methods rely on the assumption that the noise is weak enough to allow relatively long qubit coherence time under the applied control.

Here, we experimentally demonstrate a protocol for characterizing the qubit environment that overcomes the challenges arising when those assumptions are not verified. We implement the protocol using the electron spin qubit associated with a single Nitrogen-vacancy (NV) center in diamond, which has emerged as a powerful platform for quantum technologies[32,33]. The NV qubit displays a complex environment, comprising ^{13}C nuclear spins randomly distributed in the diamond lattice. The thermal and quantum fluctuations of this environment, and the distribution of environment-qubit interaction strengths make this an extremely rich scenario where
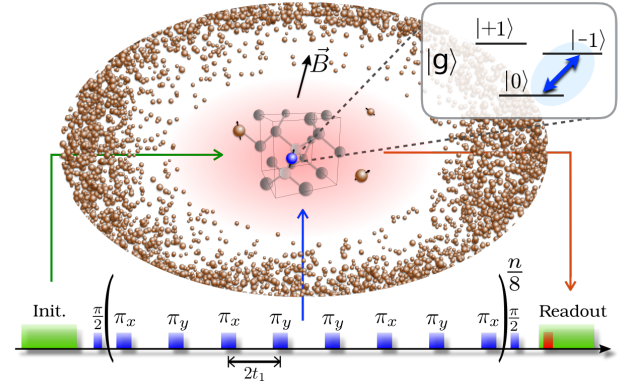

FIG. 1. **System-environment model and experimental protocol.** The NV electronic spin (blue sphere) is sensitive to ^{13}C impurities in the diamond (brown spheres), including isolated nearby spins and a larger ensemble spin bath. The NV is addressed and manipulated via optically-detected magnetic resonance in the presence of an external bias magnetic field, aligned with the NV axis. After optical initialization in the $m_s = 0$ spin state, the NV is manipulated with resonant microwave pulses (in blue), and read out optically (red). A detailed description of our experimental setup can be found in[1,30,31].

to test our protocol. The environment can be divided into a small set of resolved ^{13}C, and a large ensemble of unresolved ^{13}C that we treat as a collective bath (Fig. 1). We can further tune the ratio between the environment internal energy and its coupling to the NV center by varying the strength of an applied external magnetic field, thus exploring different bath regimes[22].

Crucially for quantum devices, we show that the acquired knowledge of a classical (weakly-coupled) bath can reliably predict the qubit dynamics even under drivings that differ from the ones used for noise spectroscopy. Conversely, we find that the assumption of one simple classical model describing an intrinsically quantum bath, strongly coupled to the qubit, is not always appropriate to achieve a predictive model for all dynamics. Instead, distinct classical models of the spin
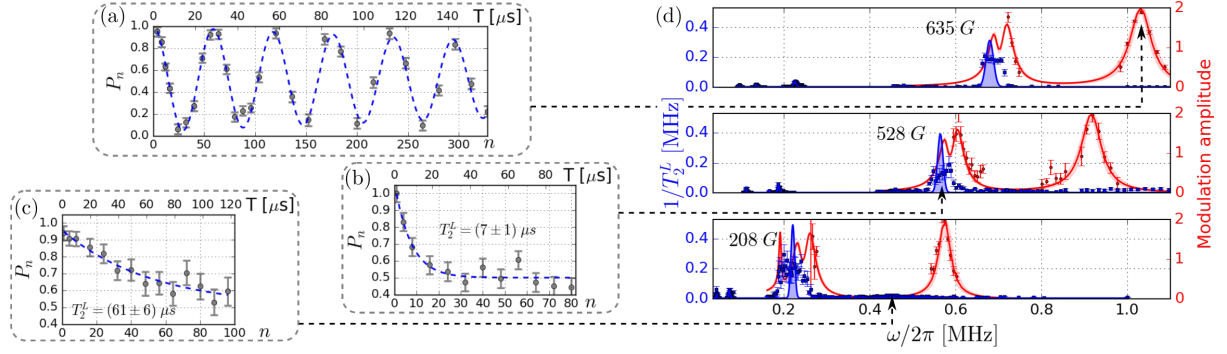
FIG. 2. (a-c) Spin coherence, mapped onto population P_n, as a function of n. The inter-pulse delay time t_1 is fixed: (a) $t_1 = 242$ ns, $B = 635$ G; (b) $t_1 = 456$ ns, $B = 528$ G; (c) $t_1 = 585$ ns, $B = 208$ G. (d) NSD and coupling with nearby nuclei. We report $1/T_2^L$ (blue, left-hand side vertical scale) and the amplitude of the observed coherent modulations (red, right-hand side vertical scale), for different magnetic field strengths ($B = 208 - 635$ G). Blue lines are the fit of high-order harmonics to extract the NSD, and red lines are the simulations of the completely resolved nearby Carbons (see text). The red shadow describes the uncertainty on the estimation of the coupling strength components. The coupling strength to the third carbon is too weak to be distinguishable from the 0th-order collapse, thus it has been extracted from higher-order harmonics (see Fig. III.S[31]).

bath are needed to predict the qubit spin behavior under different control schemes, reflecting that the bath feels the qubit back action, which varies with the control sequences driving the qubit dynamics.

II. EXPERIMENTAL SYSTEM

We investigate the environment of a single deep NV center in an electronic-grade bulk diamond (Element6), with nitrogen concentration $[^{14}N] < 5$ ppb, and natural abundance of ^{13}C (nuclear spin $I = 1/2$). In the presence of a static bias field B aligned along the NV axis, we can restrict the description to an NV spin subspace, $\{|0\rangle, |-1\rangle\}$. The system-environment Hamiltonian is

$$\mathcal{H} = \omega_0 \sigma_z^{(NV)} + \frac{\omega_L}{2} \sum_k \sigma_z^{(k)} + \hbar \sum_k \sigma_z^{(NV)} \cdot \omega_h^{(k)} \cdot \sigma^{(k)}, \quad (1)$$

where $\omega_0 = \gamma_e B$ and $\omega_L = \gamma_n B$, with γ_e and γ_n being the electron and nuclear gyromagnetic ratios, and $\omega_h^{(n)}$ the hyperfine-interaction frequency tensor. The last term incorporates a small set of discrete couplings that can be fully resolved, as later shown, and a broad unresolved distribution of couplings that we describe as a collective bath. In the strong coupling regime, where the typical coupling strength overcomes the environment internal energy ($\|\omega_h\| \geq \omega_L$), the creation of entanglement between spin qubit and a large environment, with subsequent tracing over of the environment, induces loss of qubit coherence. In the weak coupling limit, $\|\omega_h\| \ll \omega_L$, the environment can be modeled as a classical stochastic field, as described in the Supplemental Material[31], also leading to a non-unitary qubit dynamics (dephasing).

To characterize the spin environment, we reconstruct the environment-induced NV dynamics under sets of resonant multipulse control[14,15]. The control field acting on the spin qubit can be described by a modulation function $y_n(t)$ and its squared Fourier transform defines the filter function $Y_n(\omega)$[21].

Due to the presence of the bath, coherence decays as $W(t) = e^{-\chi(t)}$, where $\chi(t)$ depends on the noise spectral density (NSD) $S(\omega)$, as

$$\chi(t) = \int \frac{d\omega}{\pi\omega^2} S(\omega) |Y(\omega)|^2. \quad (2)$$

To measure $S(\omega)$, we perform a systematic spectral analysis of coherence under DD sequences of equispaced π pulses, with increasing number of pulses. We use the XY-8 sequence[34] as a base cycle (Fig. 1), as it is designed to improve robustness against detuning and imperfections of the π-pulse shape. The DD sequences are incorporated in a Ramsey interferometer that maps residual coherence after n pulses into the observable population of the $|-1\rangle$ state, $P_n = (1 + W)/2$.

III. ENVIRONMENT SPECTROSCOPY

Collective bath. For long enough evolution time (*i.e.*, large number of pulses n), equispaced sequences with interpulse delay $2t_1$ are well described by narrow monochromatic filters given by δ-functions centered at $\omega = \pi/2t_1$. In this limit, χ depends only on the NSD spectral weight at that specific frequency, whereas all nearby noise components are filtered out. Then, varying the number of pulses at fixed t_1 the coherence is expected to show an exponential decay, with a generalized coherence time T_2^{L}[14]

$$W(nt_1) = \exp\left(-\frac{2nt_1}{T_2^L}\right) \quad \text{with} \quad S(\pi/2t_1) \simeq \frac{\pi^2}{8\,T_2^L}. \quad (3)$$

The decay is faster for t_1 corresponding to the spin bath characteristic frequencies (coherence collapses), as shown in Fig. 2 (b-c). Then, a practical protocol would be to map out T_2^L varying t_1 around the first collapse, a region that carries the most information about the NSD. Fig. 2(d) shows $1/T_2^L$ as a function of $\omega = \pi/2t_1$ (blue dots).
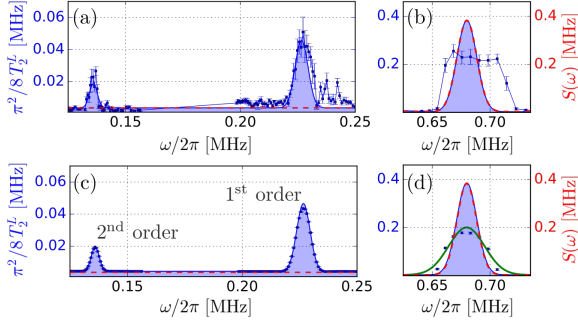
FIG. 3. $1/T_2^L$ and $S(\omega)$. (a-b) Dots are experimental $1/T_2^L$ values peaked (a) at $\omega_L/5$ ($l = 1$) and $\omega_L/3$ ($l = 2$), and (b) at ω_L ($l = 0$), with $B = 635(1)$ G. The blue line is a Gaussian fit of harmonics $l = 1, 2$, from which we extract $S(\omega)$ (red dashed line, peaked at ω_L). (c-d) Reconstruction of a model NSD, used to proof self-consistency of the method. The blue squares are $1/T_2^L$ values resulting from the fit of the simulated coherence. The solid lines are the Gaussian fits to the harmonics of orders $l = 1, 2$ (blue) and $l = 0$ (green). The red dashed line is the original model NSD.

However, a strongly-coupled spin bath may lead to very fast decay (already at $n < 8$) for t_1 around the first collapse, so that using large number of pulses is not possible. Unfortunately, for low number of pulses the filter induces an additional broadening of the NSD. Since a sequence of equidistant π pulses acts on the spin evolution as a step modulation function $y_n(t)$ with periodic sign switches, the filter function $Y_n(\omega)$ is not a single δ-function, but shows periodic sinc-shaped peaks at frequency $\omega_l = (2l + 1)\omega$, which can be well approximated by a periodic comb of δ-functions only for large n. Then, $T_2^L(\omega)$ is affected not only by $S(\omega)$, but also by its higher harmonics[14,15],

$$\frac{1}{T_2^L(\omega)} = \frac{8}{\pi^2} \sum_{l=0}^{\infty} \frac{1}{(2l + 1)^2} S(\omega_l), \qquad (4)$$

giving the approximation in Eq. 3 for $l = 0$.

This last observation gives us a simple tool to overcome the limitation of the short coherence decay time in the collapses time windows: We center the higher order harmonics of the filter function around the expected NSD peak and combine the information from several harmonics. This partially attenuates strong noise that would saturate the coherence decay and achieves a better approximation to a δ-function, as for fixed number of pulses, the filter function gets narrower at higher orders.

To validate our protocol, we simulate $W(nt_1)$ under a simple noise model (a Gaussian centered at $\omega_L = 2\pi \times 750$ kHz), and verify that $1/T_2^L$ obtained from the 0th-order filter harmonics ($l = 0$) exhibits significant disagreement with the original spectrum, whereas the $l = 1, 2$ harmonics are sufficient to fully reconstruct the NSD peak (Fig. 3(c)-(d), and Table I.S[31]). In experiments, we extract the NSD lineshape from a Gaussian fit of $1/T_2^L$ around first and second order collapses (Fig. 3(a)). Figure 3(b) shows the obtained NSD lineshape (red dashed line), compared with data from the 0th-order collapse[35].

Resolved nuclear spins. The reconstruction of the NSD from a classical model fails in some narrow time windows, where the coherence presents sharp dips reaching even negative values ($P_n < 0.5$). This allows us to identify the coherent coupling of the NV spin to a local small quantum environment, which becomes visible as the equispaced DD sequences partially filter out the larger spin bath. The hyperfine interaction to single proximal nuclear spins (Eq. 1) induces different phases for the two states $|\pm\rangle = (|0\rangle \pm |1\rangle)/\sqrt{2}$ during the spin evolution time[36–38]. The residual NV spin coherence then presents coherent modulations as a function of the pulse number [Fig. 2(a)], which give information on the hyperfine coupling tensor between the NV spin and nearby nuclear spins. The modulation amplitude shows sharp peaks as a function of frequency [red dots in Fig. 2(d)], from which we can identify three different ^{13}C nuclei and obtain an estimate of the energy-conserving component of the coupling strength, $\omega_h^{\|}$[36]. By fitting the modulations with a periodic function $M_n(T)$[31] as shown in Fig. 2(a), we extract a refined estimate of the parallel and orthogonal components of the coupling strength (see Table III.S[31]). Note that we treat each coherently coupled ^{13}C spin separately, since intra-spin couplings are negligible. A more detailed analysis (see e.g. refs.[5,39]) could be used to identify as well couplings between nuclear spins if they are strong enough to affect the dynamics.

Characterizing the spin environment of a qubit is critical to achieve improved error correction protocols. One could, e.g., exploit the coherently coupled nuclear spins in the environment to create quantum error correction codes[40–43], that could be further tailored to the measured noise spectrum[3]. An alternative strategy is to optimize dynamical decoupling sequences[2,44–47], for example to allow both noise suppression and quantum sensing[1]. It is then essential to test whether the reconstructed environment model has predictive power.

IV. VALIDITY AND LIMITS OF THE CLASSICAL NOISE MODEL

Having devised a practical protocol to reconstruct the NV environment, we implement it at different magnetic field intensities, to test whether we can obtain a predictive model of the spin environment over a range of conditions where either classical or quantum properties of the bath are expected to be visible[22]. While we expect the spin bath effects on a central spin qubit to be always described by a classic noise source model[48], noise spectroscopy allows us to mark the boundary between quantum and classical regime. The bias magnetic field applied along the NV spin not only changes the NSD central frequency (^{13}C Larmor frequency ω_L), but also its properties.

In the weak coupling regime, when $R = \omega_h^{\perp}/\omega_L \ll 1$ for most nuclei, the unpolarized nuclear bath can be described as formed by classical randomly-oriented magnetic dipoles[31]. The orthogonal component of each nuclear dipole $\sigma_n^{\perp}$ undergoes Larmor precession around the external magnetic field. The coupling to the spin qubit thus assumes the form of an effective dephasing Hamiltonian $\mathcal{H} = \gamma\beta(t)\sigma_z^{NV}$ with $\beta(t)$ a
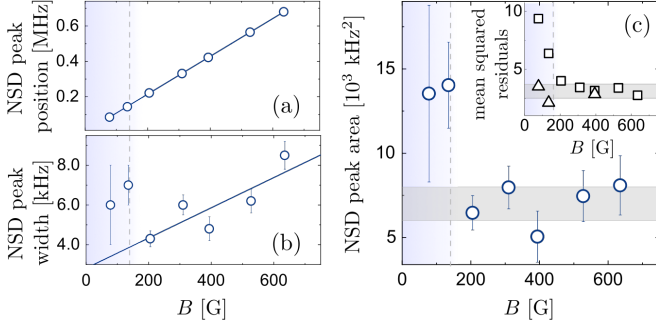
FIG. 4. NSD peak across the quantum-to-classical spin bath transition. Peak position (a), width (b), and area (c), are obtained from a Gaussian fit of the measured NSD, and reported as a function of the magnetic field strength. The blue line in (a) is a linear fit, consistent with the expected coupling frequency for a ^{13}C spin bath. The vertical dashed line represents a guide for the eye indicating a sudden change of the bath behavior – where the condition $R \gg 1$ is no longer fulfilled. The gray horizontal region in (c) denotes the mean value $\bar{A}$ and standard deviation σ of the NSD area for $B > 150$ G. Values at field $B \leq 150$ G deviate from $\bar{A}$ by $> 6\,\sigma$. Inset: mean squared residuals of the experimentally observed coherence with the simulation obtained from the measured NSD (squares) and with the 2-model simulation (triangles). Each point results from several datasets collected under different controls[31].

time-varying mean field with stochastic amplitude and phase, which can be characterized by its NSD. In Fig. 4 we plot peak center, width, and area of the measured $S(\omega)$. The center scales linearly with the magnetic field, with a slope of $1.069(2)$ kHz/G, the gyromagnetic ratio of ^{13}C (Fig. 4.a). We can ascribe the small increasing trend of the NSD width with increasing magnetic field to variations in the internal bath dynamics, as we expect more spin flip-flops at higher fields as the energy of all nuclear spins become dominated by the Zeeman energy and become energetically favorable. A detailed study of this effect, which can be included in the classical bath model, goes however beyond the scope of this work. Remarkably instead, the NSD width and area (Fig. 4(b) and Fig. 4(c)) show a discontinuity at $B \sim 150$ G, where $R \sim 1$, indicating a sudden change in the bath properties that we can associate with the boundary between the quantum and classical regimes.

Having gained in principle a full picture of the NV spin environment – noise spectrum of the bath and coherent interaction with nearby impurities, we want to confirm this to be a predictive model of the spin evolution under different kinds of time-dependent control, beyond monochromatic filters. We thus use the measured spectrum and hyperfine couplings to simulate the spin coherence under other kind of DD sequences, and we compare this prediction to measurements.

We calculate the residual coherence after a given n-pulse sequence, P_n, as due to both the spin bath and the $m = 3$ observed strongly-coupled single spins,

$$P_n(T) = \frac{1}{2}\left(1 + e^{-\chi_n(T)}\prod_{i=1}^{m} M_n^{(i)}(T)\right). \quad (5)$$

Here, $\chi_n(T)$ is obtained from the measured NSD, whereas

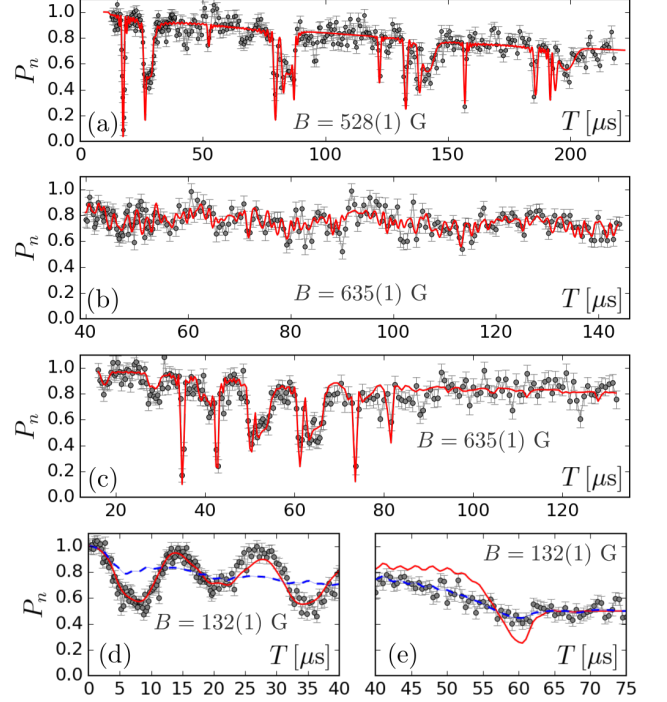$M_n(T)$ is extracted by evolving the spin under conditional evolution operators[31].

FIG. 5. **Time evolution of spin coherence under different DD sequences.** Dots are experimental data with statistical error. Red lines are the predicted coherence simulated using the measured environment, with no free parameters. (a) Four repetitions of XY-8 ($n = 32$). (b) UDD with $n = 32$. (c) AXY-8, with $n = 40$ pulses at positions $t_{ij} = \frac{T}{80}(10i + j - 8)$, with $i = 1...8$ and $j = 1...5$[31]. (d-e) Low-field results for (d) spin-echo and (e) Uhrig $n = 32$. The blue dashed line is obtained from the NSD best fit to a set of multipulse sequences (Uhrig, AXY-4, and AXY-8). Mean squared residuals of the experiments with simulation are summarized in the inset of Fig.4(c).

Figure 5 compares simulation and experimental P_n. In addition to equispaced sequences, such as spin echo and XY8-N used for noise spectroscopy, we implemented Uhrig dynamical decoupling (UDD[2]), which was recently used to detect remote nuclear spin pairs[39], as it highly suppresses the effect of coupling to single nearby nuclei; and adaptive XYN sequences, AXY-N[49], which have been proposed to improve the robustness and discrimination of single nuclear spins.

At high field, the excellent agreement between data and simulations (see also inset of Fig. 4(c), squares) demonstrates that the spin bath can be described independently of the NV dynamics, since the coupling of the NV center to the spin bath can be neglected compared to the bath internal energy. In the strong-coupling regime, at $B \leq 150$ G, we expect the bath dynamics to be modified by the controlled NV dynamics due to the back action of the NV onto the bath itself. In other words, one single classical model is no longer suitable to describe the bath when the NV dynamics is driven by different kinds of DD sequences. We observe indeed that the NSD measured with equispaced sequences does not predict correctly the measured coherence independently of the applied control. However, since the NV spin is a simple two-level system, once

fixed the control sequence acting on the NV spin we should be able to find a classical model of the spin bath[48] (we note that we still can correctly model the contribution from the coherently coupled nuclear spins using the same parameters and Hamiltonian as in the high-field regime). We find that two classical noise spectra are enough to achieve predictive results (Fig. 5 (d,e), and inset of Fig. 4(c)). The NSD extracted with the method described in Sec. III correctly describes the coherence for DD sequences with small n numbers (e.g. Hahn echo in Fig. 5 (d)). On the other hand, the spin dynamics under sequences with a large number of pulses can be predicted by an alternative NSD line shape, obtained from the simultaneous fit of P_n under different multi-pulse controls, which fails in turn to predict Hahn echo (Fig. 5 (d,e)). The two line shapes differ from each other significantly[31], but this combined two-model picture well describes the spin behavior under all the explored controls (inset of Fig. 4(c), triangles).

V. CONCLUSIONS

We have experimentally demonstrated a method to spectrally characterize the nuclear spin environment of NV centers, even when the resulting NV coherence time is short. The environment comprised both nearby nuclei, that induce coherent modulations, as well as a larger ensemble of nuclear spins, which we aim to model with a classical bath. Our method allows identifying the characteristic parameters of both components of the environment (Hamiltonian of nearby nuclei and NSD of the bath). The reconstruction of the full environment model can be then used to predict the NV coherence even when the spin dynamics is driven by different kinds of control.

In a weak coupling regime, at high magnetic fields, the environment model fully predicts the measured spin coherence under various control sequences. At low magnetic fields, where the quantum dynamics of the nuclear spin bath is expected to have larger influence, still we can always identify a classical noise model describing the NV central spin decoherence, even if decoherence is fundamentally induced by the nuclear spin bath via entanglement with the NV center. However, due to the control-driven qubit back action on the bath, the classical noise model is not generally predictive, and we find that different environment models are needed to describe the evolution under different types of applied controls.

By studying the validity and limits of a robust environment characterization protocol, able to address a complex quantum environment and provide a simplified (classical) model, our results pave the way to more robust quantum devices, protected by noise-tailored error correction techniques.

* fabbri@lens.unifi.it

[1] F. Poggiali, P. Cappellaro, and N. Fabbri, Phys. Rev. X **8**, 021059 (2018).

[2] G. S. Uhrig, Phys. Rev. Lett. **98**, 100504 (2007).

[3] D. Layden and P. Cappellaro, npj Quantum Information **4**, 30 (2018).

[4] G. Goldstein, P. Cappellaro, J. R. Maze, J. S. Hodges, L. Jiang, A. S. Sorensen, and M. D. Lukin, Phys. Rev. Lett. **106**, 140502 (2011).

[5] M. H. Abobeih, J. Cramer, M. A. Bakker, N. Kalb, M. Markham, D. J. Twitchen, and T. H. Taminiau, Nature Communications **9** (2018).

[6] A. Cooper, W. K. C. Sun, J.-C. Jaskula, and P. Cappellaro, arXiv:1807.00828 (2018).

[7] B. A. Myers, A. Das, M. C. Dartiailh, K. Ohno, D. D. Awschalom, and A. C. Bleszynski Jayich, Phys. Rev. Lett. **113**, 027602 (2014).

[8] T. Rosskopf, A. Dussaux, K. Ohashi, M. Loretz, R. Schirhagl, H. Watanabe, S. Shikata, K. M. Itoh, and C. L. Degen, Phys. Rev. Lett. **112**, 147602 (2014).

[9] T. van der Sar, F. Casola, R. Walsworth, and A. Yacoby, Nat. Commun. **6**, 7886 (2015).

[10] A. Stark, N. Aharon, T. Unden, D. Louzon, A. Huck, A. Retzker, U. L. Andersen, and F. Jelezko, Nat. Commun. **8**, 1105 (2018).

[11] J. Bylander, S. Gustavsson, F. Yan, F. Yoshihara, K. Harrabi, G. Fitch, D. G. Cory, and W. D. Oliver, Nat. Phys. **7**, 565 (2011).

[12] C. Belthangady, N. Bar-Gill, L. M. Pham, K. Arai, D. Le Sage, P. Cappellaro, and R. L. Walsworth, Phys. Rev. Lett. **110**, 157601 (2013).

[13] I. Almog, Y. Sagi, G. Gordon, G. Bensky, G. Kurizki, and N. Davidson, J. Phys. B: At., Mol. Opt. Phys. **44**, 154006 (2011).

[14] T. Yuge, S. Sasaki, and Y. Hirayama, Phys. Rev. Lett. **107**, 170504 (2011).

[15] G. A. Álvarez and D. Suter, Phys. Rev. Lett. **107**, 230501 (2011).

[16] S. Kotler, N. Akerman, Y. Glickman, A. Keselman, and R. Ozeri, Nature **473**, 61 (2011).

[17] K. C. Young and K. B. Whaley, Phys. Rev. A **86**, 012314 (2012).

[18] L. Viola and S. Lloyd, Phys. Rev. A **58**, 2733 (1998).

[19] L. Cywiński, R. M. Lutchyn, C. P. Nave, and S. DasSarma, Phys. Rev. B **77**, 174509 (2008).

[20] L. Faoro and L. Viola, Phys. Rev. Lett. **92**, 117905 (2004).

[21] M. J. Biercuk, A. C. Doherty, and H. Uys, J. of Phys. B **44**, 154002 (2011).

[22] F. Reinhard, F. Shi, N. Zhao, F. Rempp, B. Naydenov, J. Meijer, L. T. Hall, L. Hollenberg, J. Du, R.-B. Liu, and J. Wrachtrup, Phys. Rev. Lett. **108**, 200402 (2012).

[23] N. Bar-Gill, L. Pham, C. Belthangady, D. Le Sage, P. Cappellaro, J. Maze, M. Lukin, A. Yacoby, and R. Walsworth, Nat. Commun. **3**, 858 (2012).

[24] Y. Romach, C. Müller, T. Unden, L. J. Rogers, T. Isoda, K. M. Itoh, M. Markham, A. Stacey, J. Meijer, S. Pezzagna, B. Naydenov, L. P. McGuinness, N. Bar-Gill, and F. Jelezko, Phys. Rev. Lett. **114**, 017601 (2015).

[25] F. Yoshihara, Y. Nakamura, F. Yan, S. Gustavsson, J. Bylander, W. D. Oliver, and J.-S. Tsai, Phys. Rev. B **89**, 020503 (2014).

[26] S. Kotler, N. Akerman, Y. Glickman, and R. Ozeri, Phys. Rev. Lett. **110**, 110503 (2013).

[27] J. T. Muhonen, J. P. Dehollain, A. Laucht, F. E. Hudson, R. Kalra, T. Sekiguchi, K. M. Itoh, D. N. Jamieson, J. C. McCallum, A. S. Dzurak, and A. Morello, Nat Nano **9**, 986 (2014).

[28] G. A. Paz-Silva and D. A. Lidar, Scientific Reports **3**, 1530 (2013).

[29] G. A. Álvarez and D. Suter, Phys. Rev. A **84**, 012320 (2011).

[30] F. Poggiali, P. Cappellaro, and N. Fabbri, Phys. Rev. B **95**, 195308 (2017).

[31] *See Supplemental Material [URL], which includes also Refs.*[50–58].

[32] M. W. Doherty, N. B. Manson, P. Delaney, F. Jelezko, J. Wrachtrup, and L. C. Hollenberg, Physics Reports **528**, 1 (2013).

[33] L. Rondin, A. Tetienne, T. Hingant, J. F. Roch, M. P., and V. Jacques, Reports on Progress in Physics **77**, 056503 (2014).

[34] T. Gullion, D. B. Baker, and M. S. Conradi, J. Mag. Res. **89**, 479 (1990).

[35] We attribute the extra broadening of 0th-order experimental data, compared with simulation, to the presence of the least-strongly-coupled among the observed nearby nuclei. This Carbon is clearly visible in higher-order harmonics, while is not resolved in the 0th-order collapse, where induces an overestimation of the NSD width.

[36] T. H. Taminiau, J. J. T. Wagenaar, T. van der Sar, F. Jelezko, V. V. Dobrovitski, and R. Hanson, Phys. Rev. Lett. **109**, 137602 (2012).

[37] S. Kolkowitz, Q. P. Unterreithmeier, S. D. Bennett, and M. D. Lukin, Phys. Rev. Lett. **109**, 137601 (2012).

[38] N. Zhao, J. Honert, B. Schmid, M. Klas, J. Isoya, M. Markham, D. Twitchen, F. Jelezko, R.-B. Liu, H. Fedder, and J. Wrachtrup, Nat. Nanotech. **7**, 657 (2012).

[39] N. Zhao, J.-L. Hu, S.-W. Ho, J. T. K. Wan, and R. B. Liu, Nat. Nanotech. **6**, 242 (2011).

[40] M. Hirose and P. Cappellaro, Nature **532**, 77 (2016).

[41] J. Cramer, N. Kalb, M. A. Rol, B. Hensen, M. S. Blok, M. Markham, D. J. Twitchen, R. Hanson, and T. H. Taminiau, Nature Communications **7**, 11526 (2016).

[42] H. Taminiau, J. Cramer, T. van der Sar, V. Dobrovitski, and R. Hanson, Nat Nano **9**, 171 (2014).

[43] G. Waldherr, Y. Wang, S. Zaiser, M. Jamali, T. Schulte-Herbruggen, H. Abe, T. Ohshima, J. Isoya, J. F. Du, P. Neumann, and J. Wrachtrup, Nature **506**, 204 (2014).

[44] H. Qi, J. P. Dowling, and L. Viola, Quantum Information Processing **16**, 272 (2017).

[45] M. J. Biercuk, H. Uys, A. P. VanDevender, N. Shiga, W. M. Itano, and J. J. Bollinger, Nature **458**, 996 (2009).

[46] G. Quiroz and D. A. Lidar, Phys. Rev. A **88**, 052306 (2013).

[47] D. Farfurnik, A. Jarmola, L. M. Pham, Z. H. Wang, V. V. Dobrovitski, R. L. Walsworth, D. Budker, and N. Bar-Gill, Phys. Rev. B **92**, 060301 (2015).

[48] D. Crow and R. Joynt, Phys. Rev. A **89**, 042123 (2014).

[49] J. Casanova, Z.-Y. Wang, J. F. Haase, and M. B. Plenio, Phys. Rev. A **92**, 042304 (2015).

[50] L. Childress, M. V. Gurudev Dutt, J. M. Taylor, A. S. Zibrov, F. Jelezko, J. Wrachtrup, P. R. Hemmer, and M. D. Lukin, Science **314**, 281 (2006).

[51] A. Maudsley, Journal of Magnetic Resonance (1969) **69**, 488 (1986).

[52] W. H. Zurek, Physics Today **44**, 36 (1991).

[53] J. Helm and W. T. Strunz, Phys. Rev. A **80**, 042108 (2009).

[54] J. Helm, W. T. Strunz, S. Rietzler, and L. E. Würflinger, Phys. Rev. A **83**, 042103 (2011).

[55] W. Yang and R.-B. Liu, Phys. Rev. Lett. **101**, 180403 (2008).

[56] N. Zhao, J. Wrachtrup, and R.-B. Liu, Phys. Rev. A **90**, 032319 (2014).

[57] W. Ma, F. Shi, K. Xu, P. Wang, X. Xu, X. Rong, C. Ju, C.-K. Duan, N. Zhao, and J. Du, Phys. Rev. A **92**, 033418 (2015).

[58] A. M. Souza, G. A. Álvarez, and D. Suter, Phys. Rev. Lett. **106**, 240501 (2011).